Holmes, W. M., Vallatos, A., Gilmour, L. and Chalmers, A. J. (2018) Multiple boli arterial spin labelling for high signal-to-noise rodent brain perfusion imaging. *Magnetic Resonance in Medicine*, 79(2), pp. 1020-1030. (doi:10.1002/mrm.26706)

Multiple boli Arterial Spin Labelling for high signal-to-noise rodent brain perfusion imaging

Antoine Vallatos[a], Lesley Gilmour[b], Anthony J. Chalmers[b] & William M. Holmes[a*]

[a] Glasgow Experimental MRI Centre, Institute of Neuroscience and Psychology, University of Glasgow, UK.

[b] Wolfson Wohl Translational Cancer Research Center, Institute of Cancer Sciences, University of Glasgow, UK.

*Correspondence to: William M. Holmes, Glasgow Experimental MRI Centre, Institute of Neuroscience and Psychology, University of Glasgow, Wellcome Surgical Centre, Garscube Estate, Bearsden Road, Glasgow G61 1QH, UK (william.holmes@glasgow.ac.uk).

ABSTRACT

Purpose: A systematic method is proposed for optimising a promising preclinical arterial spin labelling (ASL) sequence based on the use of a train of adiabatic radio-frequency pulses labelling successive boli of blood water.

Methods: The sequence optimisation is performed and evaluated using brain imaging experiments in mice and in rats. It involves the investigation of several parameters, ranging from the number of adiabatic pulses and labelling duration, to the properties of the adiabatic hyperbolic secant pulses (i.e. amplitude and frequency modulation).

Results: Species dependant parameters are identified, allowing for robust fast optimisation protocols to be introduced. The resulting optimised multiple boli ASL (mbASL) sequence provides with significantly higher average signal-to-noise ratios (SNR) per voxel volume than currently encountered in ASL studies (278 mm^{-3} in mice and 172 mm^{-3} in rats). Comparing with the commonly used Flow-sensitive Alternating Inversion Recovery technique (FAIR), mbASL-to-FAIR SNR ratios reach 203 % for mice and 725 % for rats.

Conclusion: When properly optimised, mbASL can offer a robust, high SNR ASL alternative for rodent brain perfusion studies

KEY WORDS

ASL, SNR, perfusion, mouse brain, rat brain

INTRODUCTION

Arterial Spin Labelling (ASL) allows tissue perfusion to be imaged by inverting the longitudinal magnetisation of inflowing arterial blood water. Due to their ability to characterise tissue perfusion non-invasively, ASL techniques are becoming precious tools in the assessment of a wide range of pathologies(1), including stroke(2), brain tumours(3) and epilepsy(4).

ASL techniques typically divide into two categories, continuous ASL (CASL) and pulsed ASL (PASL). In CASL, flow-driven adiabatic inversion is used to continuously invert blood passing through a given plane(5). Subtraction of the labelled and unlabelled image acquisitions provides contrast between well and less well perfused regions. CASL provides efficient spin labelling(6) but this is counter-balanced by the need for an extra coil to locally apply a continuous radiofrequency (RF) pulse and by important magnetisation transfer effects at higher magnetic fields. PASL techniques avoid these limitations by using single inversion pulses with standard MRI hardware. The most commonly used types of PASL are EPISTAR(7), in which a slice-selective inversion is performed, and FAIR(8), which combines slice-selective and global inversion. Inversion in PASL sequences is typically achieved by adiabatic pulses such as the hyperbolic secant pulses (HS) introduced by Silver *et al.*(9). Here, the applied field expression is given by:

$$B_1(t) = [A_0\, sech(\beta t)]^{1+i\mu} \qquad \textit{Equation 1}$$

where A_0 is the maximum B_1 field applied, β is a modulation angular frequency and μ a dimensionless parameter. If the adiabatic condition given by $A_0 \gg \sqrt{\mu}\beta/\gamma$ is met and $\mu \geq 2$, the resulting magnetisation is essentially independent of the amplitude of the B_1 field, making the inversion insensitive to small magnetic field inhomogeneities(10). It is often convenient to describe HS pulses in a phase-modulated reference frame that varies at a constant carrier frequency ω_c. Here, HS pulses of maximum amplitude ${\omega_1}^{max}$ can be described by an amplitude modulation function,

$$\omega_1(t) = {\omega_1}^{max}\, sech(\beta t) \qquad \textit{Equation 2}$$

and a frequency modulation function.

$$\omega_{RF}(t) - \omega_c = \frac{d\varphi}{dt} = -\mu\beta\, tanh(\beta t) \qquad \textit{Equation 3}$$

Silver *et al.* (10) showed that an increase in μ produces a sharper selection profile, counterbalanced by less efficient adiabatic inversion. The authors found that efficient inversion and selectivity was obtained for $\mu = 5$, a value often used in subsequent studies seeking optimal adiabatic inversion (e.g. it is the default value of the HS inversion pulse on preclinical Bruker instruments: 'sech.inv' pulse).

Using adiabatic pulses, PASL techniques often achieve better labelling efficiency than CASL, but the continuous labelling of the latter allows for more spins to be inverted, leading to higher ASL signal

and Signal-to-Noise Ratios (SNR)(11). In recent years, different strategies by which to increase SNR without the additional hardware requirements of CASL have been investigated. The most common approach aims at reproducing a flow-driven pseudo-adiabatic inversion without additional coils. The resulting pseudo-Continuous ASL sequences (pCASL) consist of a series of short pulses, applied prior to image acquisition, mimicking the continuous flow-driven adiabatic inversion(12,13). pCASL sequences provide with higher SNR than PASL but, as CASL, are particularly sensitive to unbalanced magnetization transfer (MT) effects in labelling and control acquisitions. Modified pCASL sequences have been proposed in order to minimise such effects that cause measurement errors and reduction of the ASL signal (14).

An alternative ASL method, seeking to combine the labelling efficiency of PASL with the continuous inversion advantage of CASL, was proposed by Moffat *et al.*(15). Here, labelling is not based on flow-induced inversion, but on a train of adiabatic pulses inverting successive spin boli at the carotid level. Direct measurements in rat carotids (single-coil set up) showed that the pulses could achieve an average labelling efficiency of 0.79 (15), a similar value to the ones typically encountered in pCASL studies. To minimise magnetisation transfer effects, the adiabatic train is also applied during the control image but on the opposite side of the imaging plane and using an opposite sign gradient. In the seminal paper, the pulse sequence was referred as pseudo-continuous ASL but the envelop of the pulse train is far from that of the CASL one, since the inter-pulse delay (42-60 ms) is greater than the pulse duration (2ms). In fact, the resulting experiment could be compared to a multiple PASL, where each pulse inverts the spins of a blood water bolus. To avoid possible confusion and express the nature of the pulse sequence, this work will refer to this sequence as multiple boli ASL (mbASL). Note, that a similar approach was also proposed by Ouyang *et al.(16)* who used multiple concatenated rf pulses (~100) to produce a pseudo-continuous magnetisation transfer insensitive labelling technique (pTILT). The main difference with mbASL is that pTILT relies on non-adiabatic excitation pulses, thus providing with lower SNR compared to pseudo-continuous inversion based alternatives.

The mbASL sequence has been successfully used in several studies probing rat brain perfusion(17-19) and comparison with autoradiography showed it can provide with quantitative cerebral blood flow (CBF) maps of the brain(17). But despite promising results, no further development or optimisation studies have been performed(15). However, analysis of the sequence (Figure 1 a) enables identification of several parameters that could be subject to optimisation, ranging from the HS pulse properties to the pulse train timing. Moreover, the multiple boli model suggests a parameter dependence on the physiology of the scanned animal (e.g. carotid blood flow), hence the sequence parameters used by the authors for rats could generate variable quality results for different animal strains or be inefficient when working with other species. The applicability of the mbASL sequence to different species, MR platforms and field strengths has to be demonstrated and its conditions have yet to be provided.

The aim of the present work is to achieve a better understanding of and optimised parameters for this adiabatic train ASL experiment. It is important to recognise that mbASL performance will be defined by interplay between a wide range of parameters: the duration and inversion efficiency of the labelling pulses, the width and position of the inversion slab, the number of pulses, the inter-pulse delay, the adiabatic labelling duration and time distance from imaging. Here, a systematic optimisation of mbASL is proposed, focusing on the parameters describing the train of adiabatic pulses, including the labelling duration and post-labelling delay (*CI* and *TI*), the number of HS pulses (n_p) and their related parameters (μ and β). This is performed on two strains of mice (C57 & CD1) and one strain of rats (SD). To evaluate the benefits of the optimisation, a direct comparison is made with the commonly used PASL technique of Flow-sensitive Alternating Inversion Recovery (FAIR)(8).

METHODS

Animal preparation

Experiments were carried on C57 black mice (n = 12, weight: 23±3g), CD1 nude mice (n = 4, weight: 30±3g) and Sprague Dawley (SD) rats (n = 12, weight: 370±55g) (Charles River Laboratories).All experiments were performed in accordance with the local ethical review panel, the UK Home Office Animals (Scientific Procedures) Act 1986, and the United Kingdom National Cancer Research Institute guidelines for the welfare of animals in cancer research(20). The animals were anaesthetised in an adapted chamber with 5% isoflurane and a 3:7 O_2/N_2O ratio before being transferred to the MRI instrument.

MRI experimental setup

Experiments were performed on a Bruker Biospec Avance 7T imaging system with a 30 cm horizontal bore (Bruker, Germany). Homogeneous RF excitation was achieved using a birdcage volume resonator (diameter 72 mm, length 110 mm) and actively decoupled 4-channel phased array receive-only head surface coils were used for signal detection, with 22 mm length for mice and 35 mm length for rats (Rapid Biomedical, Germany). The system is equipped with shielded gradients producing up to 400 mT m^{-1} magnetic field gradients.

For in vivo experiments the animals were positioned prone on an adapted animal cradle and a hot water circulation jacket was used to regulate physiological temperature (36.5^oC – 37.5^oC). The head was centred and held laterally by wooden conical rods placed in the ears. Longitudinally, the head was fixed by the nose cone used for anaesthetic gas delivery. The animals breathed spontaneously using the facemask, with isoflurane delivered at a constant flow mixed with a 2:3 ratio of Os_2/N_2O (1 L min^{-1}). Isoflurane concentration was varied from 1.5 % to 3 %, in order to maintain stable respiration rates in normal physiological ranges (40-70 bpm for mice and 60-90 bpm for rats).

Respiration was monitored using a pressure sensor connected to an air-filled balloon placed under the abdomen of the animal (Biotrig software, UK).

ASL sequences

ASL experiments were performed using either the mbASL pulse sequence or the manufacturer standard Flow-sensitive Alternating Inversion Recovery (FAIR) pulse sequence (Figure 1). Image acquisition was performed using an Echo Planar Imaging (EPI) module. To allow direct comparison between the two ASL methods, identical EPI imaging parameters were used: Field of view was 1.76×1.76 cm for mice and 3×3 cm for rats, matrix size was 96×96, TR was 7 s, TE was 12 ms, 4 acquisition segments were used, the bandwidth was 200 kHz and 4 averages were used. For both methods a 1 mm thick imaging slice was used, positioned at 4 mm posterior from rhinal fissure for mice and 8 mm for rats. Note, that only first order shimming was used in order to minimise alterations of the HS pulse performances that could compromise the comparison between ASL results at different labelling positions.

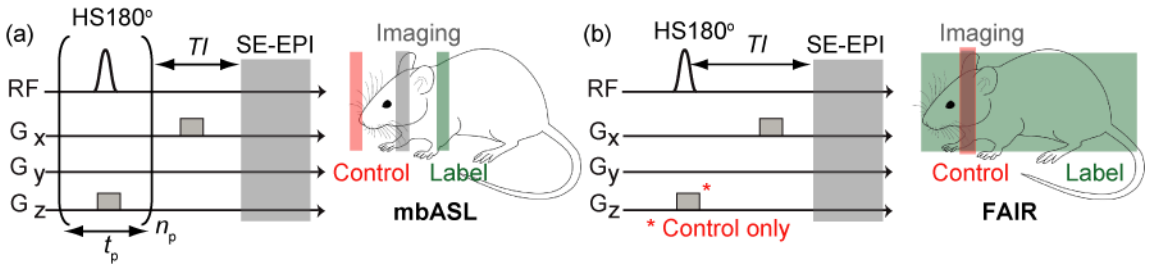

Figure 1. Pulse sequence and schematic diagram of the location of the imaging, labelling and control slices for (a) mbASL EPI and (b) FAIR EPI. Note that the homogeneous excitation region is of about 110 mm, Hence, in the case of rat experiments, non-selective rf pulses do not cover the entire animal body.

The mbASL EPI method was implemented by pre-weighting the EPI sequence with a train of slice-selective hyperbolic secant (HS) inversion pulses. The bolus width and distance from the imaging plane was chosen carefully as their interplay with the animal vascular anatomy and the homogeneity of the field and RF coil was expected to affect the sequence performance. The centre of the inversion slab was positioned close to the neck centre, 15 mm offset from imaging slice centre for mice and 30 mm offset for rats. The inversion slab width was set so as to cover most of the common carotid arteries, 8.5 mm for mice and 10.5 mm for rats. Note that for rats a relatively thinner slice was used so as to avoid the B_1 inhomogeneity regions that could affect the effective inversion of the lower RF bandwidth adiabatic pulses(21). This will increase the number of pulses necessary to achieve pseudo-continuous labelling. The continuous inversion time, $CI = n_p \times t_p$, was varied between 0.5 s and 5 s, while the delay following the pulses, *TI*, varied between 0.05 s and 5 s. The number of HS inversion pulses was varied between 1 and 70 and their duration was set to 3.3 ms. Longer HS inversion pulses

can provide with better inversion efficiency(22) but will reduce inversion efficiency on the fastest flowing spins. The HS pulses were implemented using dedicated software (Bruker TOPSPIN 2.1). The dimensionless amplitude parameter, μ, was varied between 2 and 14, while the angular modulation β was varied between 360 s^{-1} and 2520 s^{-1} (Supporting Figure S1 a), with $\mu/\beta = 1/200$ for the Bruker sech.inv . The HS pulse bandwidth range was 1-10 kHz. RF power delivered by individual HS pulses was calculated using the pulse implementation software. The approximate RF power delivered during an mbASL experiment was computed by integration of all HS pulses over the period going from the beginning of an experiment to the start of the next one. SAR was estimated as the ratio of the total RF power per kg, assuming a tissue load of 30 g for mice and 300 g for rats. For the longest pulse trains in this work, SAR ranges were of 0.7- 3.9 W/kg for mice and 0.5- 2.8 W/kg for rats, depending on the HS pulse used.

The standard FAIR EPI method present on Bruker instruments (Paravison version 5.1) was used. A 12 mm thick labelling inversion slice was situated in the centre of the imaging plane. The duration of the HS sech inversion pulse was set to 3.3 ms. The delay between inversion and image acquisition, *TI*, was 1750 ms. This was chosen in accordance with previously published optimisation studies(23)and positively evaluated by preliminary experiments in rats and mice (n = 2) by varying *TI* with 250 ms steps between 1000 ms and 2500 ms and looking for the higher SNR.

ASL data analysis

MRI data were exported in DICOM format and processed using in-house Matlab code (MathWorks Ltd., U.K.). Modified Bloch equations describe tissue magnetization *M*(t) in the presence of inflowing spins and blood flow quantification relies on subtracting two images acquired with different states for arterial blood magnetization, $\Delta M_{ASL}(t) = M_{control}(t) - M_{label}(t)$ (Figure 2 a). Regions of interest were manually selected on a control image and used for the analysis of all ASL data of a scanning session (Figure 2 b). SNR was evaluated by $SNR_{ASL} = \frac{\Delta M_{ASL}}{\sigma_M}\sqrt{2 - \frac{\pi}{2}}$, where σ_M is the noise standard deviation of the magnitude image(24).

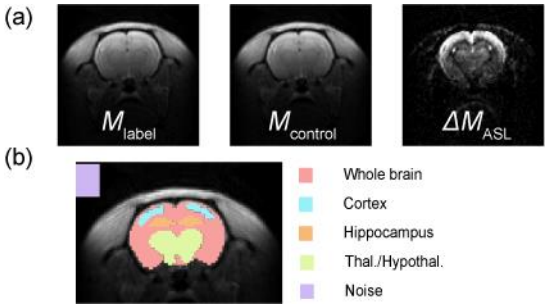

Figure 2. (a) ΔM signal in a rat brain obtained by subtracting M_{label} from $M_{control}$. (b) The regions of interest delineated on a $M_{control}$ image.

MR experiments

HS pulses ex vivo

Phantom experiments were performed in order to characterise the adiabatic inversion and slice selectivity of HS pulses and the role of HS parameters μ and β. These experiments were performed on a 20 mm diameter tube filled with a water solution doped with 1 g L^{-1} $CuSO_4$ (T_2 = 174 ms, T_1 = 359 ms). Single HS pulses were applied followed by a delay *TI* = 11 ms prior to acquisition. Inversion quality of the HS pulses, α, was evaluated by the ratio of the average signal in the inversion region to the reference signal (100% inversion) compensated for relaxation over *TI*.

Labelling duration and post-labelling delay (*CI* and *TI*)

The effects of the labelling duration (*CI*) and post-labelling delay (*TI*) on ΔM_{mbASL} were studied using a short *CI* followed by a variable *TI*: spins were inverted using five pulses (HSμ6β1080) evenly spread over 500 ms (*CI*), while *TI* was varied with 500 ms steps between 50 ms and 5000 ms.

Number of pulses (n_p)

The effect of the number of pulses on ΔM_{mbASL} was evaluated by varying the number of pulses evenly distributed along *CI*, with *TI* and *CI* fixed at 50ms and 5000 ms respectively. The n_p ranges were determined using preliminary experiments in rats and mice (n = 1). HSμ8β720 pulses were used for these experiments.

HS pulses in vivo

The effect of HS parameters μ and β on the resulting ΔM_{mbASL} was evaluated by mbASL measurements using different HS pulses. *TI* was 50 ms, *CI* was 5 s, 10 HS pulses were used for mice and 20 pulses for SD rats. Although far from reaching the phase array coil RF duty cycle limits (2.5 W), some mbASL experiments were expected to produce more hardware heating than others, possibly affecting the performance of subsequent ones. This is particularly true for experiments using high $\mu\beta$ pulses (high amplitude/modulation) that require stronger current intensities (Supporting Figure S1 b).

To minimise bias on the HS parameter evaluation, experiment ordering was randomised for each animal.

Comparison with FAIR

To evaluate the performance of the optimised mbASL, comparison was made with FAIR ASL using identical imaging parameters. *CI* was 5 s for mouse experiments and 4 s for rat experiments. For mouse experiments a train of 10 pulses was applied, while for rat experiments the number of pulses had to be adjusted: as optimal results were obtained for n_p = 70 over 5 s, for a *CI* of 4s, n_p needed to be of 56 in order to achieve the optimal inter-pulse delay t_p. These experiments were conducted in separate imaging sessions from optimisation studies, including four previously unused animals.

RESULTS

HS pulse inversion quality and slice selectivity ex vivo

Figure 3 a-b shows characteristic inversion profiles for some of the applied HS pulses, and Figure 3 c-d shows their amplitude and normalised frequency modulation (equations 2 and 3). The RF amplitude required to achieve an adiabatic inversion varied for different parameters μ and β, with low $\mu\beta$ pulses (e.g. HSμ4β360) providing poor adiabatic inversion and too low or too high modulation pulses suffering from poor inversion profiles (e.g. HSμ2β2520).

Inversion quality, α, and inversion percentages in regions 1 and 2 (defined in Figure 3 a) for all HS pulses are shown in Figure 3 e-g. Good inversion ($\alpha \geq 93.9\%$) was obtained for all pulses where $\mu \geq 4$ and $\beta \geq 720$ s^{-1}. For lower β value pulses (β = 360 s^{-1}) adiabaticity seems to be compromised as $\mu\beta$ did not reach the critical value (note that α increases with μ). For pulses with lower μ values (μ = 2), the quality of the inversion was lower, but no clear trend was observed. HS sech produced 93.9.6% inversion, while higher inversion was obtained for HSμ6β1080 (94.9%) and HSμ8β720 (94.3%).

For region 1, low $\mu\beta$ pulses produced more than 5% inversion outside the inversion plane, indicating poor slice selectivity. Except for HSμ4β720 (5%), pulses of $\mu \geq 4$ and $\beta \geq 720$ s^{-1} gave inversions below 2% in this region (sech 0.8%). For region 2, except HSμ4β360 (10%) and HSμ4β360 (4.5%), all pulses produce inversions below 2.5%, with sech (0.3%) and HSμ8β720 (0.7%) having the lower inversion percentages.

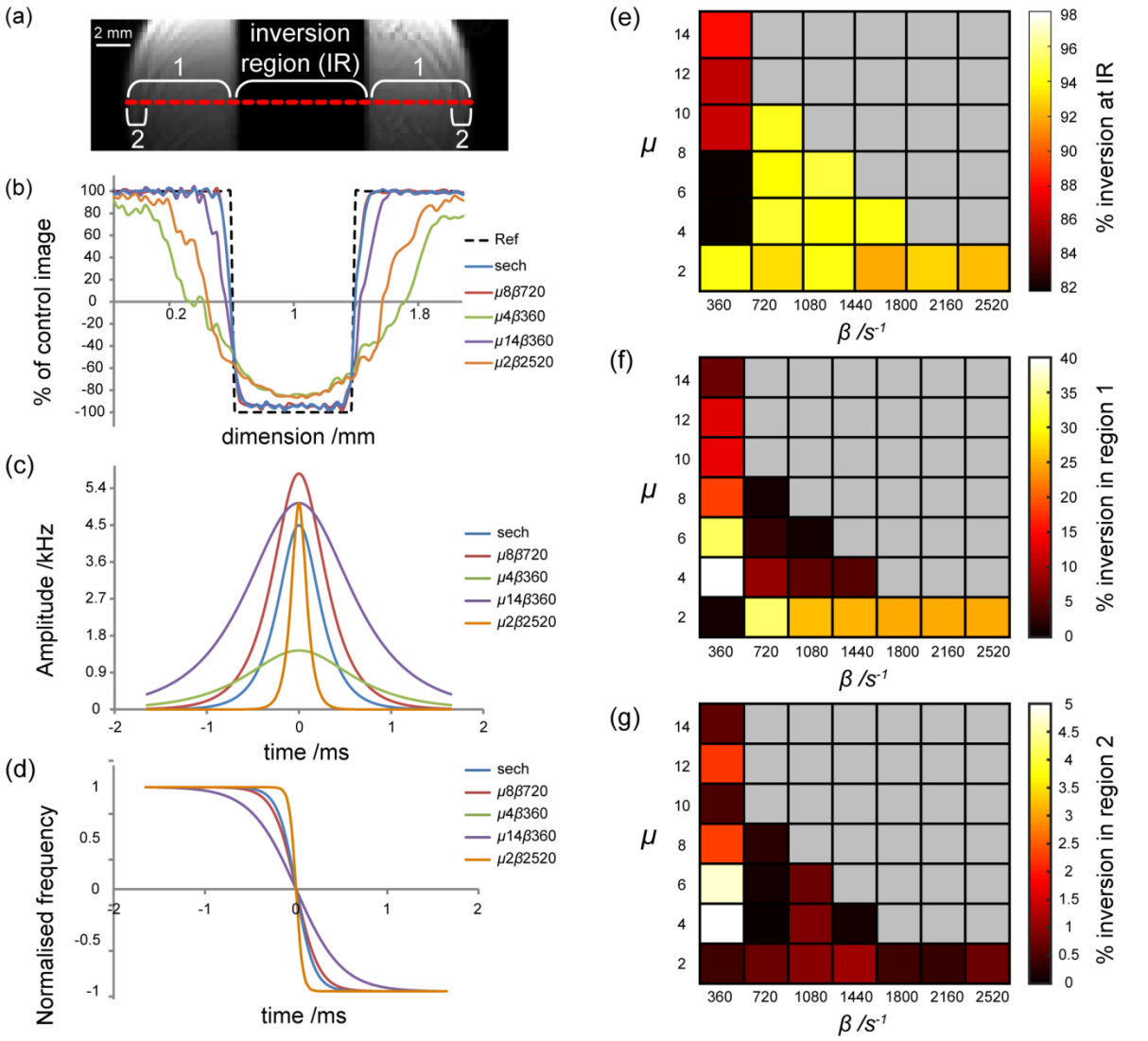

Figure 3. (a) Image of the phantom with an inverted slice of 8 mm achieved using a single HS$\mu 8\beta 720$ pulse. Inversion region and regions 1 and 2 are highlighted. (b) Normalised signal profiles along the dotted line in (a), (c) modulation of amplitude and (d) normalised frequency for different inversion pulses. (e-g) Box plots showing signal inversion percentage against HS parameters μ and β, in different regions indicated in (a): Aimed inversion region (e) and regions 1 (f) and 2 (g). The grey boxes correspond to non-measured values.

Labelling duration and post-labelling delay

Figure 4 a-b shows whole brain average $\Delta M_{\mathrm{mbASL}}$ produced by the short pulse train (5 pulses over 500 ms) for different *TI* values. Values are in percentage of the sum of the obtained $\Delta M_{\mathrm{mbASL}}$ signals for these series of experiments. This sum should approximate $\Delta M_{\mathrm{mbASL}}$ resulting from a single experiment where *CI* = 5000 ms and *TI* = 50 ms. The resulting plots give an insight into the contribution of the

pulses according to their time distance from image acquisition. Maximum $\Delta M_{\mathrm{mbASL}}$ was obtained with a *TI* of 1000 ms for mice and 500 ms for rats.

A cumulative representation of the data (Figure 4 c-d) facilitates decisions regarding the duration and the starting and ending point of the HS pulse train. In SD rat experiments, pulses applied more than 4 seconds from the image acquisition had a negligible contribution (≤ 5%) and could therefore be removed, allowing a reduction of both experimental time and specific absorption rate (SAR). This is not the case for C57 mice experiments in which significant contributions were still obtained for pulses applied 5 s before image acquisition. In both rat and mice experiments short *TI* pulses have significant contributions.

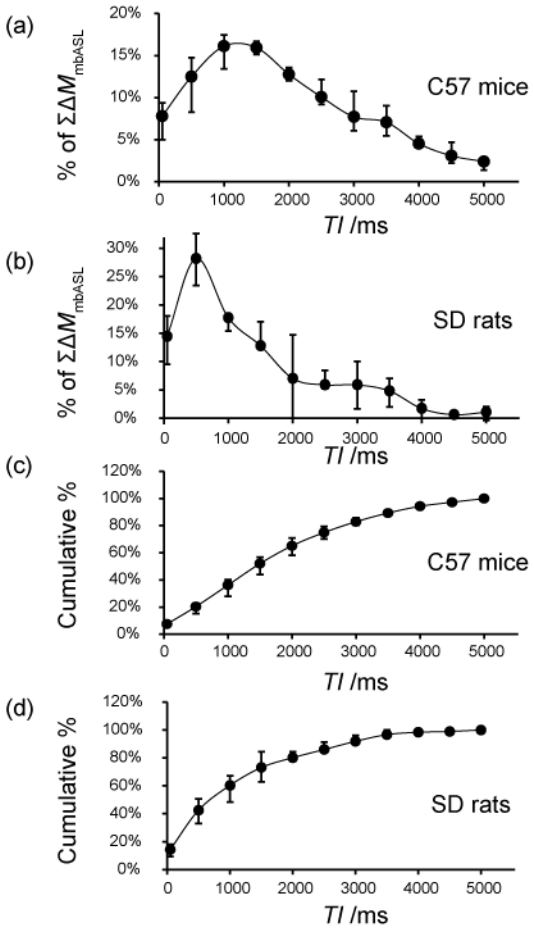

Figure 4. Signal percentage against TI for (a) C57 mice (n=5) and (b) SD rats (n=5). Cumulative signal percentage against TI for (c) C57 mice and (d) SD rats.

Number of pulses

Figure 5 a-b shows the whole brain average $\Delta M_{\mathrm{mbASL}}$ (in percentage of the maximum $\Delta M_{\mathrm{mbASL}}$) against the number of applied pulses. These plots allow identification of n_{p} values maximising

ΔM_{mbASL}, n_p = 10 for mice and n_p = 70 for SD rats. Note that for rats although the signal was still increasing at n_p = 70 the slope of the curve indicates that the maximum value is almost reached.

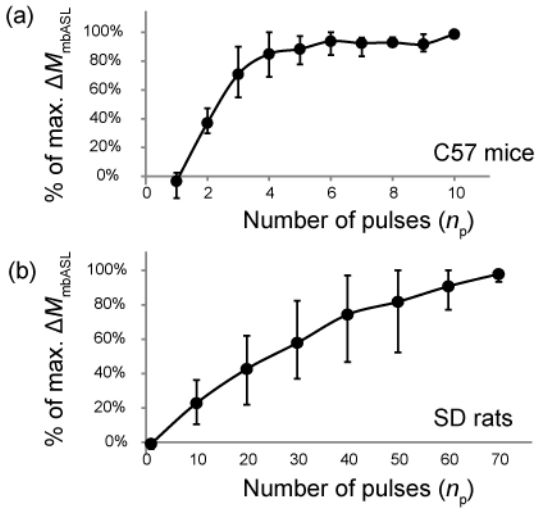

Figure 5. Percentage of maximum ΔM_{mbASL} obtained in the whole brain against number of HS pulses for (a) C57 mice (n=5) and (b) SD rats (n=5).

HS pulse parameters

Figure 6 a,c shows the resulting ΔM_{mbASL} for different HS pulses as a percentage of ΔM_{mbASL} sech. For C57 mice (n_p = 10), HSμ8β720, HSμ2b2160, HSμ6β1080 and HSμ4β1440 are the pulses with the best performances. HSμ8β720, HSμ6β1080 and HSμ4β1440 produced higher ΔM_{mbASL} than the sech pulse in each studied animal (Figure 6 b). For SD rats (n_p = 20), pulses with lower $\mu\beta$ values show better performances (HS μ4β360, HSμ2β720), probably because they tend to invert broader regions than pulses with $\mu \geq 4$ and $\beta \geq 720$ s^{-1} (i.e. worse slice selectivity) and therefore achieve higher inversion efficiency with lower n_p. Sensible comparison can be done for similar slice selectivity pulses ($\mu \geq 4$ / $\beta \geq 720$ s^{-1}), where HSμ8β720 and HSμ6β720 provided with the best performances.

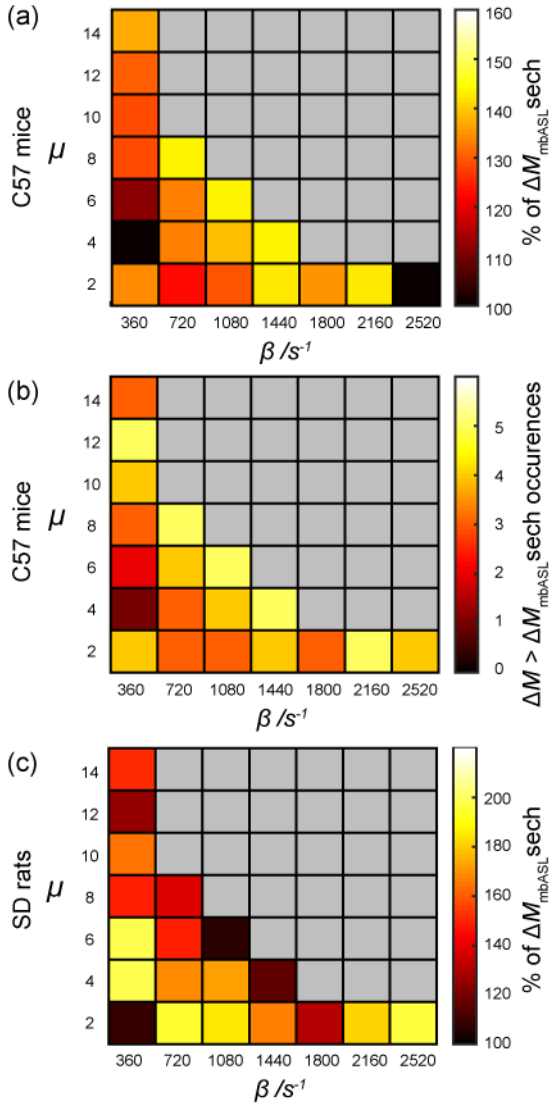

Figure 6. (a-b) Box plots showing whole brain average ΔM_{mbASL} as a percentage of ΔM_{mbASL} sech for different μ and β values: (a) C57 black mice (n =5) and (b) SD rats (n = 5). The grey boxes correspond to non-measured values due to SAR limitations (rf power increases with parameters μ and β). (c) Number of times the HS pulse gave higher ΔM_{mbASL} than sech in the C57 experiments.

Comparison with FAIR ASL

Figure 7 shows average ΔM and SNR as a percentage of ΔM_{FAIR} and SNR_{FAIR}. In mice, mbASL experiments provided at least 20% higher signal than FAIR and 60% higher SNR (Figure 7 a). The HS pulse producing the higher ΔM_{mbASL} (HSμ8β720) was also used in FAIR, providing a 10% ΔM_{FAIR} improvement. All mbASL experiments provided at least 20% higher signal than FAIR and 60% higher SNR. mbASL μ2β2520 showed the higher average performance (about 160% of ΔM_{FAIR} and

203% of SNR_{FAIR}) but poor stability, leading to a broad spread of outcomes. Considering both robustness and signal, mbASL $\mu 8\beta 720$ gave the best results, generating on average 140% of ΔM_{FAIR} signal and 191% of SNR_{FAIR}.

For rat experiments the mbASL sequences provided much better outcomes than FAIR. ΔM_{mbASL} sech and ΔM_{mbASL} $\mu 8\beta 720$ were respectively 270% and 310% of ΔM_{FAIR}. The 23-pulse mbASL $\mu 2\beta 720$ provided with 260% of FAIR signal, while the same HS pulse sequence using 56 pulses produced slightly lower outcomes, confirming the fact that above the optimal n_p no additional signal gains are expected. Note that the 23-pulse mbASL $\mu 2\beta 720$ has 92% lower SAR than mbASL sech. Overall, average SNR_{mbASL} was at least 600% of SNR_{FAIR}, with SNR_{mbASL} $\mu 8\beta 720$ being about 725% of SNR_{FAIR}. Comparison between SNR_{ASL} values per voxel volume for mice and rat experiments suggests that the difference between ASL outcomes should be mainly attributed to low SNR_{FAIR} values for the rat experiments. For example, mbASL $\mu 8\beta 720$ produced an average SNR per voxel volume of 278 mm^{-3} in mice and 172 mm^{-3} in rats, while FAIR produced 155 mm^{-3} in mice and only 26 per mm^{-3} in rats.

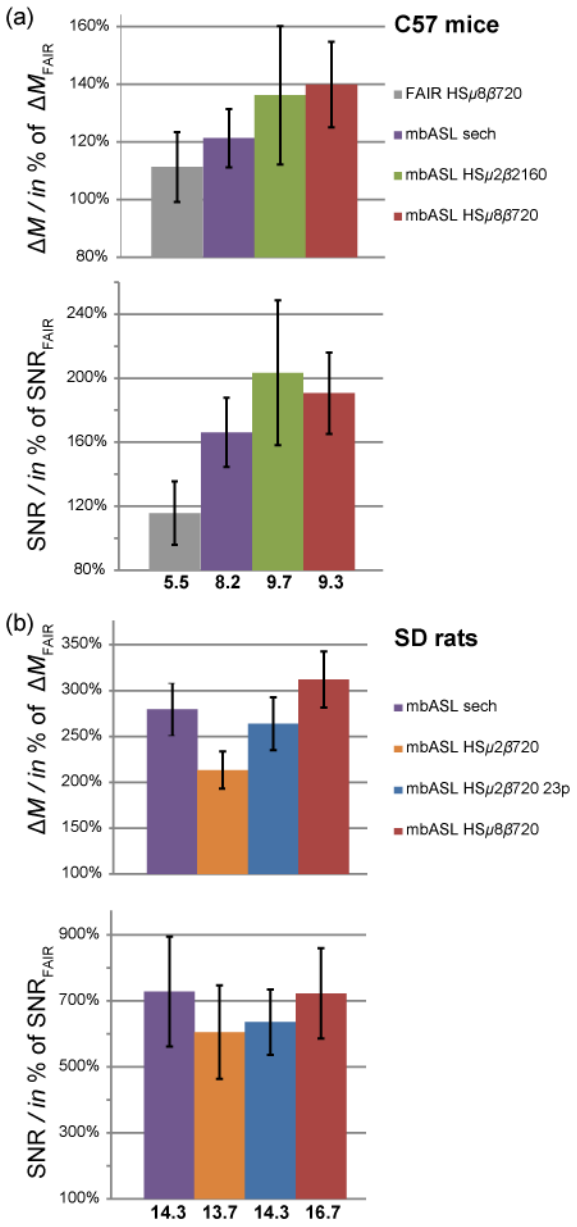

Figure 7. Average ΔM and SNR for the whole brain region as a percentage of ΔM_{FAIR} and SNR_{FAIR} (100%) for (a) C57 mice(n=7) and (b) SD rats (n=7). SNR values obtained with each ASL sequence are indicated in bold characters below each bar.

Figure 8 shows Δ*M* images from this set of experiments. To allow comparison the same image scale was used for each set of images. Post mortem images acquired with mbASL $\mu 8\beta 720$ had Δ*M* levels lower than 5% of in vivo images, confirming that non-perfusion related signal input is negligible.

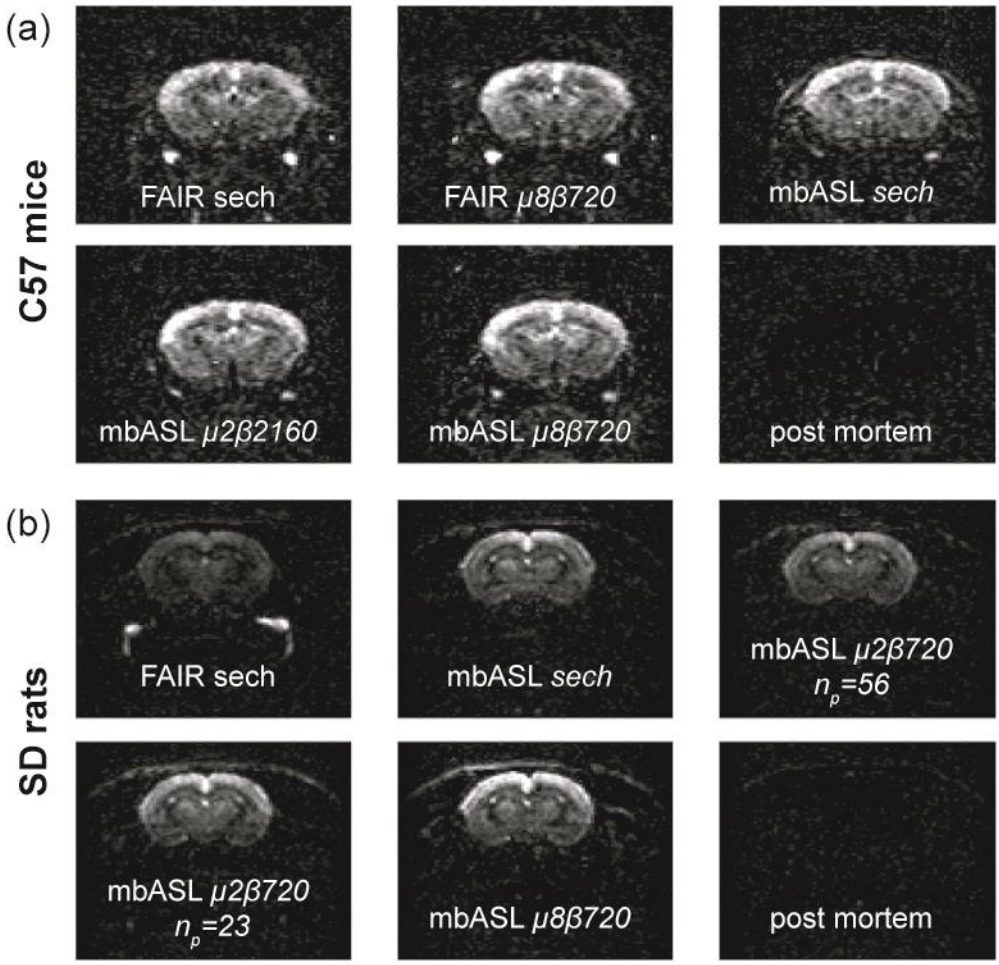

Figure 8. ΔM_{ASL} *images for C57 mice and SD rats using FAIR and mbASL sequences (4 averages). The furthest right image of each set corresponds to post mortem acquisition using mbASL μ8β720*

The quantitative nature of mbASL measurements was interrogated by comparing the ΔM distribution in different brain regions to the distribution obtained by FAIR. Figure 9 shows the relative signal in each brain region compared to the whole brain signal. Ratios above 1 correspond to regions were the average signal was higher than the average signal in the whole brain (e.g. cortical region). Note that no statistically significant ΔM distribution differences were observed between the mbASL and FAIR sequences.

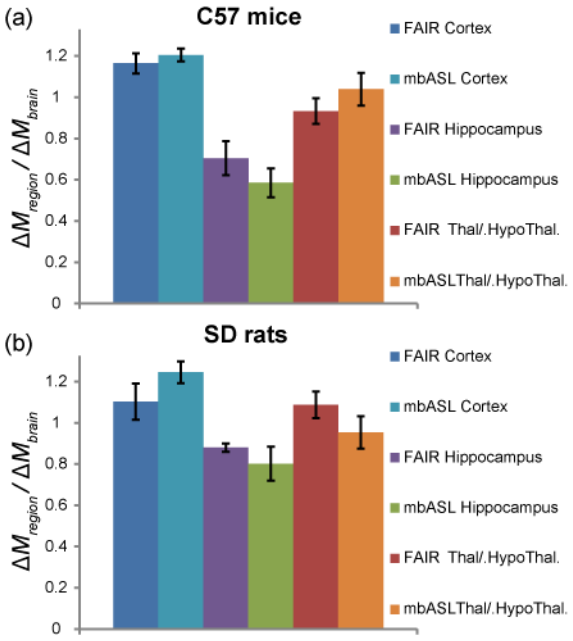

Figure 9. Ratio of the ASL signal in different brain regions (characteristic ROIs are indicated in figure 2) to the whole brain signal ($\Delta M_{region} / \Delta M_{brain}$) for (a) FAIR sech and (b) mbASL $\mu 8 \beta 720$ (n = 7).

DISCUSSION

A structured method for the optimisation of the mbASL sequence was presented, showing how successive analysis of the effects of pulse timing (*CI* and *TI*), number of HS pulses (n_p) and HS properties (affected by μ and β) enables significant improvements to be obtained for both ΔM_{mbASL} and SNR_{mbASL}.

Slice selectivity and inversion efficiency of a range of HS pulses was evaluated with single pulse mbASL experiments performed ex vivo (Figure 3). Inversion efficiency results (Figure 3 e) were in agreement with previous theoretical and experimental results on the relationship between inversion quality (α) and HS parameters μ and β (22). But the main goal of this set of experiments was to evaluate the inversion rate outside the aimed inversion region. In fact, depending on the distance between the inversion plane and the image, low slice selectivity pulses could compromise mbASL accuracy by directly labelling spins within the imaging plane. Considering that for in vivo experiments the imaging slice was set at 11 mm from the inversion slab for mice and 25 mm for rats, negligible labelling was expected on the image plane from most of the pulses in this range (Figure 3 g). Phantom experiments also enabled investigating the effect of multiple adiabatic inversions on the same spins (Supporting Figure S2), showing that a significant n_p overestimation could be detrimental for mbASL as it might lead to signal loss. This effect is expected to be negligible on the fast flowing spins considered in vivo, but might cause signal loss for slow moving blood water spins. Despite their

insight into HS pulse inversion quality and slice selectivity, phantom experiments have to be considered with caution, as only stationary water protons are considered. In vivo HS optimisation was therefore necessary in order to account for the effects of flowing blood spins in the presence of slice selection gradients(25). Note that adiabatic pulse variants, as Frequency Offset Corrected Pulses(26) (FOCI), could provide with improved inversion and slice selectivity performances while reducing RF power requirements. Although high slice selectivity is not crucial for mbASL, and SAR was evaluated below 4W/kg for all experiments in this work, these optimised adiabatic pulses could be used to produce lower SAR mbASL sequences.

The first in vivo optimisation step focused on the pulse sequence timing. Measuring the ΔM signal at different *TI* values (Figure 4 a-b) shows the contribution of each pulse in the train to the overall ASL signal. The cumulative representation (Figure 4 a-b) allowed to easily identify the labelling duration (*CI*) and post-labelling delay (*TI*) maximising $\Delta M_{\mathrm{mbASL}}$ while avoiding unnecessary pulses to be applied. Note that the results showed very similar inflow curves in all regions of the brain (Supporting Figure S3), confirming that timing optimisation applies to all brain regions.

In order to get a deeper insight into the nature of mbASL labelling, the results of Figure 4 a-b can be analysed in terms of the kinetic model proposed by Buxton *et al.*(27), where the ΔM signal is defined by the combination of magnetisation delivery by arterial flow, magnetisation clearance by venous flow and T_1 relaxation. Here, this analysis is not straightforward as one has to take into account that each point in the plots corresponds to an averaged signal coming from blood spins labelled over 500 ms. For example, in the case of rat experiments (Figure 4 b), ΔM average for $TI < 500$ ms includes low contributions from inversions with *TI* lower than the arterial transit time (200 - 400 ms) (6), hence the the signal maximum is achieved for 500 ms < *TI* < 1000 ms. In the case of mice experiments the signal maximum is achieved for higher post-labelling delays (1000 ms < *TI* < 2000 ms). This can be counter-intuitive as arterial transit times measured in mice are expected to be lower than in rats (80 ms) (28). The fact than a greater bolus temporal width is observed in mice can be explained by the use of a relatively thicker inversion slice compared to rats (probably covering part of the abdomen), in conjuction with the use of 5 successive pulses, making the plot of ΔM against *TI* look similar to ones typically observer in PASL techniques (27). Note that the maximum signal is achieved at similar *TI* to the one maximising FAIR signal (~ 1750 ms). Using the standard kinetic model allows to reproduce the data shown in Figure 4 a (Supporting Figure S4) and provide with an estimate of the arterial transit time (50-100 ms) in good agreement with previously reported data (28).

The next optimisation step was to find the number of pulses maximising $\Delta M_{\mathrm{mbASL}}$ (Figure 5). Using large inversion slabs allows reducing the optimal n_{p} (and lower SAR) but introduces analysis complications, as inversion boli cover more of the rodent circulatory system than just the carotid artery. Nevertheless, a simple bolus model, where the number of pulses is related to the average blood

velocity (V), inversion slab length (L) and labelling duration (CI) provides useful insight into these results. In such model, the optimal n_p is given by the ratio of CI to the time necessary to refill the inversion region following a pulse (t_p), $n_p=CIV/L$. With same CI and similar L values for mouse and rat experiments (8.5 mm and 10.5 mm respectively) n_p optimisation was expected to strongly depend on average blood velocities. This allows to explain the fact that much higher optimal n_p values were encountered in rats where the blood flow(29) can be several times higher than in mice(30). Further analysis also indicates a relationship between n_p and the animal weight (Supporting Figure S5), with larger animals requiring higher n_p. The correlation was much stronger in the case of rats, which allows explaining why the used n_p range was slightly lower than necessary to reach the ASL signal plateau (Figure 5 b): parameter ranges were defined with preliminary experiments carried at earlier time points on animals from the same batch that had lower weight, hence achieving maximum signal at lower n_p values.

Following optimisation of labelling timing and number of pulses, the in vivo performance of HS pulses was investigated. As discussed, in and ex vivo performances are expected to differ, since for in vivo experiments pulses are applied off-resonance(31) and on flowing spins(32,33). Moreover, Garcia *et al.*(22) showed that lower inversion performances are encountered when inverting blood water rather than tissue spins, which they attributed to magnetisation transfer effects. But in vivo pulse optimisation results (Figure 6) must also be considered with precaution, as cerebral blood flow variations over the course of the experiments may modulate the outcome of the results. For mbASL experiments on mice, where the n_p maximising ΔM_{mbASL} was used, the HS pulses giving the higher ΔM_{mbASL} were the same as the ones giving the higher inversion in the phantom experiments (e.g. HS$\mu 8\beta 720$). The main difference was identified in the low $\mu\beta$ pulses providing with much lower outcomes in vivo. For the rat experiments where a lower n_p value than the one maximising ΔM_{mbASL} was used, low $\mu\beta$ pulses provided higher ΔM_{mbASL} (e.g. HS$\mu 4\beta 360$). Robustness was also considered in order to identify stable outcome HS pulses, as a high average ΔM_{mbASL} does not ensure satisfactory performances for each scan. In a basic approach, robustness was evaluated by the number of times a pulse gave outcomes better than the standard sech pulse.

Different optimal mbASL parameters were found for C57 mice and SD rats, with the greatest differences seen in the optimal number of pulses. To further investigate this subject dependence, we performed additional experiments on four CD1 nude mice. The CI, TI and HS parameters were fixed to the values that maximised ΔM_{mbASL} in the C57 black mice experiments (CI = 5 s, TI = 50 ms, HS$\mu 8\beta 720$). The higher ΔM_{mbASL} values in CD1 mice were obtained for $12 \leq n_p \leq 20$ where the sequence performance plateaus before starting to drop for n_p = 24 (Supporting Figure S6). The average weight and length of CD1 mice is greater than C57 mice, hence a slightly larger optimal n_p was to be expected. This stresses the need to optimise mbASL for the species and strains being

studied and suggests that identifying the n_p maximising ΔM_{mbASL} provides with a fast optimisation protocol.

Comparison with FAIR (Figure 7) showed that the mbASL sequence offers significant increase both in ΔM (about 140% of ΔM_{FAIR} in mice and 360% in rats) and SNR (about 200% of ΔM_{FAIR} in mice and 700% in rats). The high mbASL performances observed in rats were partly attributed to low FAIR performances. In fact, due to the short length of volume resonators used in pre-clinical systems, only the upper body of larger animals fits within the homogenous region of the resonator, with low lower body experiencing reduced B_1 fields. Thus, not all blood water in the body is efficiently inverted, leading to a reduced ASL signal. By using slice-selective inversion closer to the head, mbASL and pCASL sequences have an advantage over FAIR. From this set of data HS$\mu 8\beta 720$ appears to be the optimal pulse in the studied range for both mice and rat experiments, providing similar slice selectivity to sech pulse, with better inversion performance in vivo and 50% lower SAR. Note that HS $\mu 8\beta 720$ also allowed to increase FAIR signal (Figure 7 a). The optimised mbASL $\mu 8\beta 720$ sequence provided with an average SNR of 9.3 for 0.034 mm^3 voxels in mice and 16.7 for 0.098 mm^3 voxels in rats. Although it is difficult to compare results obtained on different setups and parameters, those SNR values seem greater than the ones typically encountered in most preclinical and clinical PASL/pCASL studies (16,34,35). An indirect comparison between mbASL, CASL and pCASL can be made using their relative SNR performances compared to FAIR. To minimise experimental bias caused by partial body labelling of FAIR in rats, this comparison has to focus on C57 mice data. While CASL SNR is 2.7 times higher than PASL in theory, it is only 30-50% in practice (11), while results in mice reported 50% SNR improvement for pCASL compared to FAIR (36). These are to be compared with 91% higher SNR than FAIR achieved by the optimised mbASL $\mu 8\beta 720$ sequence. Note that the labelling performances of mbASL are expected to be similar for different species (e.g. rats), as the use of adiabatic pulse inversion makes it less sensitive to flow variations than flow induced inversion sequences.

Finally, the optimised mbASL was shown to provide with proportional ΔM distribution in the brain to FAIR (Figure 9), showing that relative perfusion measurements were achieved and reinforcing previous studies demonstrating the quantitative nature of mbASL perfusion measurements in comparison with autoradiography (17). Further CBF analysis of mbASL data was not included, assuming that parameter variations involved in the present study were not significantly affecting CBF quantification. This allowed eliminating additional inversion recovery scans, increasing available scanning time per animal and favouring a wider analysis of mbASL parameter effects. Nevertheless, results highlighting the hybrid PASL/CASL nature of mbASL (Figure 4 a-b) have to be considered carefully in order to achieve accurate CBF quantification. For example, quantification using PASL equations might be more accurate when a relatively thick labelling plane is used (e.g. C57 mice

experiments). Quantitative CBF maps using the pCASL equations should be achievable when using a relatively thin labelling plane (e.g. SD rat experiments). This analysis suggests that mbASL CBF values will be situated within the range of CBF measurement discrepancies observed between PASL and CASL techniques (37).

CONCLUSIONS

This work showed that high-SNR mbASL experiments could be achieved via a comprehensive optimisation protocol adjusting the sequence parameters to the studied species. Better understanding of mbASL properties allowed envisaging paths for further improvements. For example, a systematic study of HS pulse duration effects should lead to additional signal enhancement (22). Moreover, strategies to lower power deposition were introduced so as to address SAR limitations that could occur where high n_p values compared to the animal weight are required to maximise SNR (e.g. use lower adiabaticity HS pulses or alternative adiabatic pulses). Overall, this work demonstrated that, when properly optimised, the multiple adiabatic pulse mbASL can offer a robust, high SNR ASL alternative for rodent brain perfusion studies.

Note: Supporting information is available in the online version of the paper.

ACKNOWLEDGEMENTS

This work was funded by The Brain Tumour Charity (grant ref. 26/160). The authors would also like to thank Mr James Mullin and Mrs Lindsay Gallagher for their advice and fruitful discussions on animal setup and scanning protocols.

REFERENCES

1. Detre JA, Wang JJ, Wang Z, Rao HY. Arterial spin-labeled perfusion MRI in basic and clinical neuroscience. Curr Opin Neurol 2009;22(4):348-355.
2. Chalela JA, Alsop DC, Gonzalez-Atavales JB, Maldjian JA, Kasner SE, Detre JA. Magnetic resonance perfusion imaging in acute ischemic stroke using continuous arterial spin labeling. Stroke 2000;31(3):680-687.
3. Noguchi T, Yoshiura T, Hiwatashi A, Togao O, Yamashita K, Nagao E, Shono T, Mizoguchi M, Nagata S, Sasaki T, Suzuki SO, Iwaki T, Kobayashi K, Mihara F, Honda H. Perfusion imaging of brain tumors using arterial spin-labeling: Correlation with histopathologic vascular density. Am J Neuroradiol 2008;29(4):688-693.

4. Wolf RL, Alsop DC, Levy-Reis I, Meyer PT, Maldjian JA, Gonzalez-Atavales J, French JA, Alavi A, Detre JA. Detection of mesial temporal lobe hypoperfusion in patients with temporal spin labeled lobe epilepsy by use of arterial perfusion MR imaging. Am J Neuroradiol 2001;22(7):1334-1341.
5. Sardashti M, Schwartzberg DG, Stomp GP, Dixon WT. Spin-Labeling Angiography of the Carotids by Presaturation and Simplified Adiabatic Inversion. Magn Reson Med 1990;15(2):192-200.
6. Williams DS, Detre JA, Leigh JS, Koretsky AP. Magnetic-Resonance-Imaging of Perfusion Using Spin Inversion of Arterial Water. P Natl Acad Sci USA 1992;89(1):212-216.
7. Edelman RR, Siewert B, Darby DG, Thangaraj V, Nobre AC, Mesulam MM, Warach S. Qualitative Mapping of Cerebral Blood-Flow and Functional Localization with Echo-Planar Mr-Imaging and Signal Targeting with Alternating Radio-Frequency. Radiology 1994;192(2):513-520.
8. Kim SG. Quantification of Relative Cerebral Blood-Flow Change by Flow-Sensitive Alternating Inversion-Recovery (Fair) Technique - Application to Functional Mapping. Magn Reson Med 1995;34(3):293-301.
9. Silver MS, Joseph RI, Hoult DI. Highly Selective Pi/2 and Pi-Pulse Generation. J Magn Reson 1984;59(2):347-351.
10. Silver MS, Joseph RI, Hoult DI. Selective Spin Inversion in Nuclear Magnetic-Resonance and Coherent Optics through an Exact Solution of the Bloch-Riccati Equation. Phys Rev A 1985;31(4):2753-2755.
11. Wong EC, Buxton RB, Frank LR. A theoretical and experimental comparison of continuous and pulsed arterial spin labeling techniques for quantitative perfusion imaging. Magn Reson Med 1998;40(3):348-355.
12. Dai WY, Garcia D, de Bazelaire C, Alsop DC. Continuous Flow-Driven Inversion for Arterial Spin Labeling Using Pulsed Radio Frequency and Gradient Fields. Magn Reson Med 2008;60(6):1488-1497.
13. Wu WC, Fernandez-Seara M, Detre JA, Wehrli FW, Wang J. A theoretical and experimental investigation of the tagging efficiency of pseudocontinuous arterial spin labeling. Magn Reson Med 2007;58(5):1020-1027.
14. Nezamzadeh M, Matson GB, Young K, Weiner MW, Schuff N. Improved Pseudo-Continuous Arterial Spin Labeling for Mapping Brain Perfusion. J Magn Reson Imaging 2010;31(6):1419-1427.
15. Moffat BA, Chenevert TL, Hall DE, Rehemtulla A, Ross BD. Continuous arterial spin labeling using a train of adiabatic inversion pulses. J Magn Reson Imaging 2005;21(3):290-296.

16. Cheng OY, Sutton BP. Pseudo-Continuous Transfer Insensitive Labeling Technique. Magn Reson Med 2011;66(3):768-776.
17. Baskerville TA, McCabe C, Weir CJ, Macrae IM, Holmes WM. Noninvasive MRI measurement of CBF: evaluating an arterial spin labelling sequence with Tc-99m-HMPAO CBF autoradiography in a rat stroke model. J Cerebr Blood F Met 2012;32(6):973-977.
18. Holmes WM, Lopez-Gonzalez MR, Gallagher L, Deuchar GA, Macrae IM, Santosh C. Novel MRI detection of the ischemic penumbra: direct assessment of metabolic integrity. Nmr Biomed 2012;25(2):295-304.
19. Reid E, Graham D, Lopez-Gonzalez MR, Holmes WM, Macrae IM, McCabe C. Penumbra detection using PWI/DWI mismatch MRI in a rat stroke model with and without comorbidity: comparison of methods. J Cerebr Blood F Met 2012;32(9):1765-1777.
20. Workman P, Aboagye EO, Balkwill F, Balmain A, Bruder G, Chaplin DJ, Double JA, Everitt J, Farningham DAH, Glennie MJ, Kelland LR, Robinson V, Stratford IJ, Tozer GM, Watson S, Wedge SR, Eccles SA, Navaratnam V, Ryder S, Inst NCR. Guidelines for the welfare and use of animals in cancer research. Brit J Cancer 2010;102(11):1555-1577.
21. Wells JA, Siow B, Lythgoe MF, Thomas DL. The importance of RF bandwidth for effective tagging in pulsed arterial spin labeling MRI at 9.4T. Nmr Biomed 2012;25(10):1139-1143.
22. Garcia DM, Duhamel G, Alsop DC. Efficiency of inversion pulses for background suppressed arterial spin labeling. Magn Reson Med 2005;54(2):366-372.
23. Cho JH, Cho G, Song Y, Lee C, Park BW, Lee CK, Kim N, Park SB, Kang JS, Kang MR, Kim HM, Kim YR, Cho KS, Kim JK. Feasibility of FAIR Imaging for Evaluating Tumor Perfusion. J Magn Reson Imaging 2010;32(3):738-744.
24. Gudbjartsson H, Patz S. The Rician Distribution of Noisy Mri Data. Magn Reson Med 1995;34(6):910-914.
25. Gullberg GT, Simons MA, Wehrli FW. A Mathematical-Model for Signal from Spins Flowing during the Application of Spin-Echo Pulse Sequences. Magn Reson Imaging 1988;6(4):437-461.
26. Ordidge RJ, Wylezinska M, Hugg JW, Butterworth E, Franconi F. Frequency offset corrected inversion (FOCI) pulses for use in localized spectroscopy. Magn Reson Med 1996;36(4):562-566.
27. Buxton RB, Frank LR, Wong EC, Siewert B, Warach S, Edelman RR. A general kinetic model for quantitative perfusion imaging with arterial spin labeling. Magn Reson Med 1998;40(3):383-396.
28. Chugh BP, Bishop J, Zhou YQ, Wu J, Henkelman RM, Sled JG. Robust method for 3D arterial spin labeling in mice. Magn Reson Med 2012;68(1):98-106.

29. Garciavillalon AL, Roda JM, Alvarez F, Gomez B, Dieguez G. Carotid Blood-Flow in Anesthetized Rats - Effects of Carotid Ligation and Anastomosis. Microsurg 1992;13(5):258-261.
30. Schiffers PMH, Henrion D, Boulanger CM, Colucci-Guyon E, Langa-Vuves F, van Essen H, Fazzi GE, Levy BI, De Mey JGR. Altered flow-induced arterial remodeling in vimentin-deficient mice. Arterioscl Throm Vas 2000;20(3):611-616.
31. Yongbi MN, Yang YH, Frank JA, Duyn JH. Multislice perfusion imaging in human brain using the C-FOCI inversion pulse: Comparison with hyperbolic secant. Magn Reson Med 1999;42(6):1098-1105.
32. Zhan W, Gu H, Silbersweig DA, Stern E, Yang YH. Inversion profiles of adiabatic inversion pulses for flowing spins: the effects on labeling efficiency and labeling accuracy in perfusion imaging with pulsed arterial spin-labeling. Magn Reson Imaging 2002;20(6):487-494.
33. Frank LR, Wong EC, Buxton RB. Slice profile effects in adiabatic inversion: Application to multislice perfusion imaging. Magn Reson Med 1997;38(4):558-564.
34. Kober F, Duhamel G, Cozzone PJ. Experimental comparison of four FAIR arterial spin labeling techniques for quantification of mouse cerebral blood flow at 4.7 T. Nmr Biomed 2008;21(8):781-792.
35. Fujiwara Y, Kimura H, Miyati T, Kabasawa H, Matsuda T, Ishimori Y, Yamaguchi I, Adachi T. MR perfusion imaging by alternate slab width inversion recovery arterial spin labeling (AIRASL): a technique with higher signal-to-noise ratio at 3.0 T. Magn Reson Mater Phy 2012;25(2):103-111.
36. Duhamel G, Callot V, Tachrount M, Alsop DC, Cozzone PJ. Pseudo-continuous arterial spin labeling at very high magnetic field (11.75 T) for high-resolution mouse brain perfusion imaging. Magn Reson Med 2012;67(5):1225-1236.
37. Chen YF, Wang DJJ, Detre JA. Test-Retest Reliability of Arterial Spin Labeling With Common Labeling Strategies. J Magn Reson Imaging 2011;33(4):940-949.

Multiple boli Arterial Spin Labelling for high signal-to-noise rodent brain perfusion imaging - Supporting material

Supporting Figure S1. (a) Integral of the amplitude modulation as a percentage of a similar duration door shape for different HS pulse μ and β values.(b) Rf Amplitude attenuation of HS pulses in an SD rat experiment load, for different HS μ and β values. In this scale, the values vary from 100 dB (minimum amplitude) to -6 dB (maximum amplitude). The system manufacturer (Bruker, Germany) pre-set sech pulse had the near maximal amplitude peak (-5.4 dB attenuation).

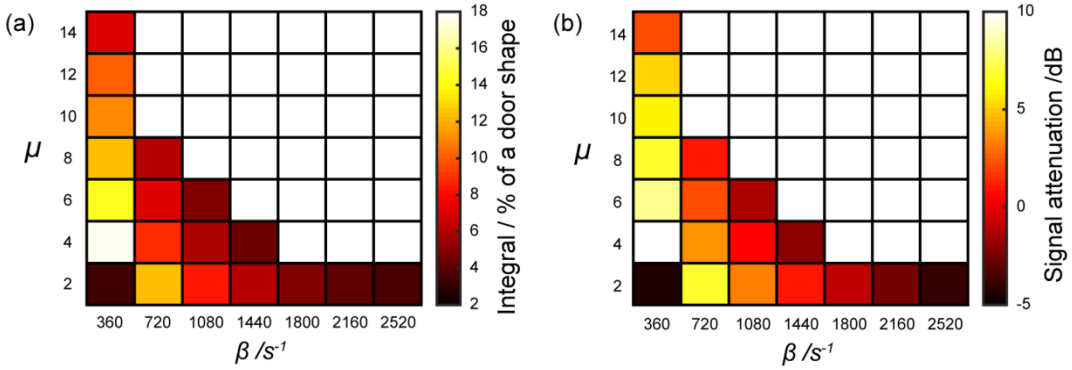

Supporting Figure S2. Phantom experiments: Inversion percentage in the inversion region as a function of the number of pulses applied over a 5s period. This can be considered as the combined effects of adiabatic inversion pulses on non-equilibrium spin systems and magnetisation transfer.

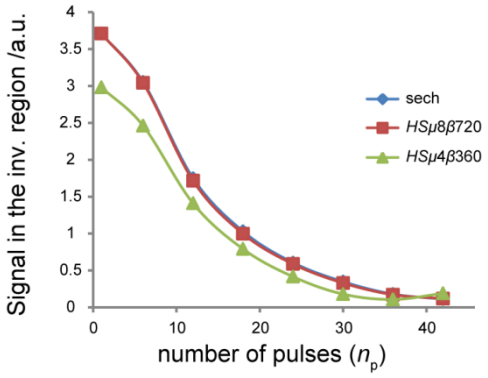

Supporting Figure S3. Average ΔM_{mbASL} against TI measured in different regions on interest for (a) C57 black mice and (b) SD rats. The similarity of the plots suggests that timing optimisation performed on whole brain ASL signal analysis will be valid for each brain region.

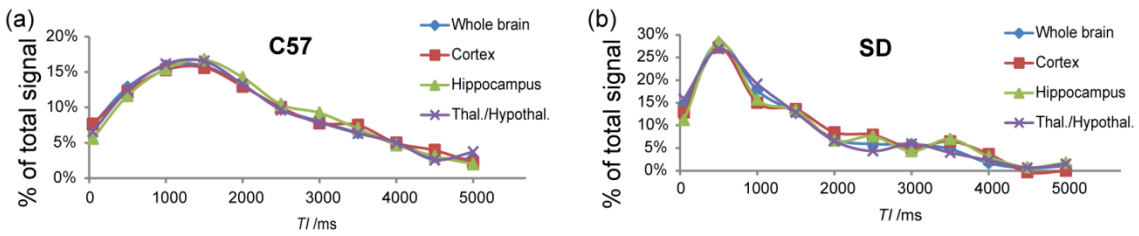

Supporting Figure S4. The solution of the standard kinetic model for the particular case of FAIR techniques (valid for arterial transit times superior to the post labelling delay, $\delta < TI$) is:

$$\Delta M^{\mathrm{FAIR}} = 2\frac{M_{\mathrm{b}}^{0}}{\lambda}\left(1 - \mathrm{e}^{-\frac{RT}{T_{1\mathrm{a}}}}\right)\cdot f \cdot \alpha \cdot \frac{\mathrm{e}^{-\frac{\delta}{T_{1\mathrm{a}}}}}{\frac{1}{T_{1\mathrm{app}}} - \frac{1}{T_{1\mathrm{a}}}} \cdot \left(\mathrm{e}^{-\frac{TI-\delta}{T_{1\mathrm{a}}}} - \mathrm{e}^{-\frac{TI-\delta}{T_{1\mathrm{app}}}}\right)$$

Where ΔM^{FAIR} is the ASL signal, M_b^0 the blood magnetisation, T_{1a} the T_1 relaxation value of blood, T_{1app} the T_1 relaxation value of tissue, f the cerebral blood flow, α the inversion efficiency, λ the blood tissue partition function, δ the arterial transit time, RT the recovery time and TI the post labelling delay.

This equation was used to calculate the expected ΔM signal distribution for different TI and δ values with $M_b^0 = 1$, $T_{1a} = 1.8$ s, $T_{1app} = 1.5$ s, $\alpha = 0.79$, $\lambda = 0.9$, $f = 1$ ml/g/min and RT = 7s. (a) Normalised ΔM against TI for different arterial transit times (50 ms $< \delta <$ 500 ms). (b) ΔM against TI, where the values of 5 successive points of (a) (spread over 500 ms) were averaged to simulate the cumulative signal from 5 pulses. The results are presented as a percentage of the sum of ΔM signals over this range of TIs.

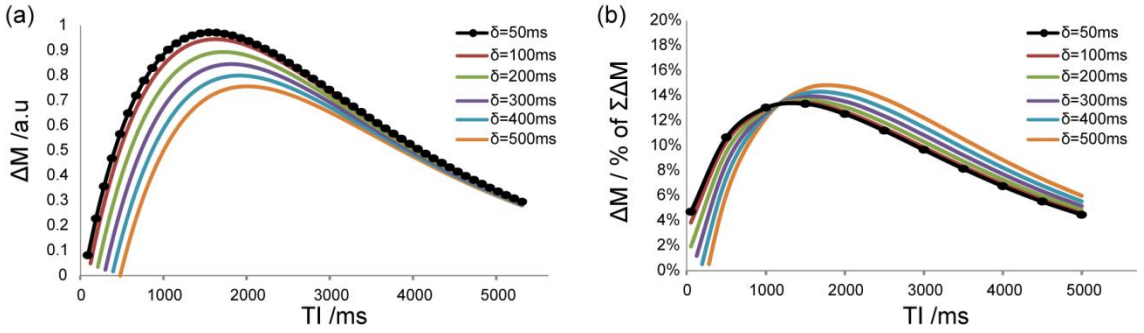

Supporting Figure S5. Number of pulses maximising ΔM_{mbASL} against animal weight for (a) C57 mice and (b) SD rats. For C57 mice, where weight variation was small and the slab thickness large, no clear trend could be found, but in the case of SD rats it clearly appeared that bigger animals required higher number of pulses. This is in agreement with the multiple boli model as the same thickness inversion slab will cover bigger region of a smaller animal.

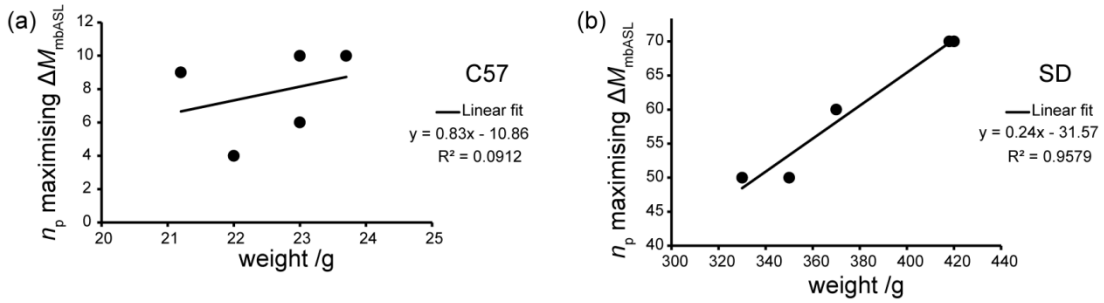

Supporting Figure S6. (a)Percentage of maximum ΔM_{mbASL} (HSμ8β720) as a function of the number of pulses for CD1 mice (n=4). (b) ASL images for CD1 mice using FAIR and mbASL μ8β720. On the four scanned animals ΔM increase using mbASL was of 16.5%, 20.4% , 36.2% and 48.6%, giving an average of 30.5%.